Mechanical regulation of vascular growth and tissue regeneration in vivo

Joel D. Boerckel[a], Brent A. Uhrig[a], Nick J. Willett[a], Nathaniel Huebsch[b], and Robert E. Guldberg[a,1]

[a]Institute for Bioengineering and Bioscience, Woodruff School of Mechanical Engineering, Georgia Institute of Technology, 315 Ferst Drive, Atlanta, GA 30332; and [b]School of Engineering and Applied Sciences, Wyss Institute of Biologically Inspired Engineering, Harvard University, 29 Oxford Street, Cambridge, MA 02138

Edited by Antonios Mikos, Rice University, Houston, TX, and accepted by the Editorial Board August 2, 2011 (received for review May 7, 2011)

New vascular network formation is a critical step in the wound healing process and a primary limiting factor in functional tissue regeneration. Like many tissues, neovascular networks have been shown in vitro to be highly sensitive to mechanical conditions; however, the effects of matrix deformations on neovascular network formation and remodeling in engineered tissue regeneration in vivo have not been evaluated. We quantified the effects of early and delayed functional loading on neovascular growth in a rat model of large bone defect regeneration using compliant fixation plates that were unlocked to allow transfer of ambulatory loads to the defect either at the time of implantation (early), or after 4 wk of stiff fixation (delayed). Neovascular growth and bone regeneration were quantitatively evaluated 3 wk after the onset of loading by contrast-enhanced microcomputed tomography and histology. The initial vascular response to bone injury featured robust angiogenesis and collateral vessel formation, increasing parameters such as vascular volume and connectivity while decreasing degree of anisotropy. Application of early mechanical loading significantly inhibited vascular invasion into the defect by 66% and reduced bone formation by 75% in comparison to stiff plate controls. In contrast, delaying the onset of loading by 4 wk significantly enhanced bone formation by 20% and stimulated vascular remodeling by increasing the number of large vessels and decreasing the number of small vessels. Together, these data demonstrate the mechanosensitivity of neovascular networks and highlight the capacity of biomechanical stimulation to modulate postnatal vascular growth and remodeling.

tissue engineering | regenerative medicine

New vascular network formation is critical for tissue regeneration and wound healing, and is a primary limiting factor in the engineering of functional tissues (1, 2). Cellular differentiation and matrix synthesis are strongly influenced by perturbations in local biomechanical conditions, a regulatory mechanism that appears to be conserved across multiple types of tissues (3–5). Bone cells, for example, are highly mechanosensitive and coordinate to adaptively remodel surrounding matrix (6). Likewise, endothelial cells and vascular networks respond dynamically in vitro to mechanical stimuli, including both fluid shear stress and mechanical strain (7–10). The material properties of the surrounding extracellular matrix have also been shown to affect the process of angiogenesis (11).

In vitro studies on the effects of external mechanical stimulation on neovascular network formation and remodeling suggest that the effects depend on the surrounding environment and stimulus magnitude. For example, Mooney and colleagues demonstrated that 6% cyclic uniaxial strain increased endothelial cell tube formation and angiogenic growth factor secretion for cells cultured in two dimensions (2D), whereas in 3D culture, 8% strain regulated the directionality of the neovascular networks, but diminished new branch formation (5, 8). Others have shown that mechanical stretch alters the orientation of 3D microvascular networks without significantly affecting endothelial sprouting (9, 10). Wilson et al. found disruption of endothelial network formation but increased production of proangiogenic proteins in response to 2.5% strain (12). These observations demonstrate the mechanosensitivity of engineered vascular networks in vitro and suggest that one mechanism by which mechanical conditions may modulate tissue regeneration is via regulation of postnatal neovascular network formation; however, little is known about the effects of functional loading on neovascular network formation during tissue regeneration in vivo.

Bone healing, for example, requires neovascular growth (13). Most bone fractures go on to heal with minimal surgical intervention (14); however, traumatic bone and soft tissue injuries that require tissue-engineered regeneration of large tissue volumes are plagued by neovascular deficiency due to the large defect size and associated nutrient diffusion limitations (15, 16). Mechanical conditions may be important regulators of postnatal neovascular network formation and tissue regeneration, which may provide a potential point of intervention to enhance vascularized tissue repair.

In this study, we examined the effects of functional, in vivo mechanical loading on neovascular growth and subsequent tissue regeneration in the context of recombinant human bone morphogenetic protein-2 (rhBMP-2)-mediated repair of large segmental bone defects in a rat model. We hypothesized that in vivo mechanical loading modulates neovascular growth and tissue formation as a function of the timing of load application. We therefore quantitatively assessed the effects of both early (immediate onset) and delayed (week 4 onset) loading on vascular growth and remodeling and subsequent bone formation. We found that early loading disrupted nascent vessel formation and vascular ingrowth, resulting in impaired regeneration, whereas delayed loading stimulated vascular network remodeling, and enhanced regeneration of functional engineered tissue.

Results

Vascular Response to Injury. We used a previously characterized 8-mm rat femoral bone defect model to evaluate the effects of in vivo loading on vascular growth and tissue regeneration (17–20). Bone defects were treated with the osteogenic growth factor rhBMP-2, delivered in an alginate-based system that provided spatiotemporal control over protein delivery (18–20), and stabilized with either stiff or compliant fixation plates (Fig. S1) that could be unlocked to allow transfer of loads caused by ambulation to the regenerating tissues (21). In the unlocked configuration, the compliant plates allowed transfer of compressive loads along the bone axis, but prevented twisting and bending of the limbs.

Author contributions: J.D.B. and R.E.G. designed research; J.D.B., B.A.U., N.J.W., and R.E.G. performed research; N.H. contributed new reagents/analytic tools; J.D.B., B.A.U., N.J.W., and R.E.G. analyzed data; and J.D.B. and R.E.G. wrote the paper.

The authors declare no conflict of interest.

This article is a PNAS Direct Submission. A.M. is a guest editor invited by the Editorial Board.

[1]To whom correspondence should be addressed. E-mail: robert.guldberg@me.gatech.edu.

This article contains supporting information online at www.pnas.org/lookup/suppl/doi:10.1073/pnas.1107019108/-/DCSupplemental.

The stiff and locked compliant plates limited all modes of load transfer (21). Bone formation and vascular structures were quantified at week 3 after plate unlocking by contrast-enhanced microcomputed tomography (microCT) (22) as described in *Materials and Methods*. Overall, the massive injury resulted in a rapid and extensive angiogenic response in the surrounding tissues, with collateral vessel formation and growth of blood vessels toward the site of injury (Fig. 1 and Fig. S2). This study evaluated the ability of early and delayed mechanical loading to modulate the growth and remodeling of these neovascular networks.

Effects of Early Mechanical Loading. To evaluate the effects of early loading, compliant fixation plates were implanted in the unlocked configuration to allow ambulatory load transfer from day zero. Defects in the early loading groups and their contralateral stiff plate controls ($n = 9$–10 per group) received either 0.5 or 2.5 μg rhBMP-2, chosen based on a previous dose-response study (19). Two doses were selected: one that induces bone formation, but fails to induce consistent bridging of the defects (0.5 μg), and one that induces robust bone formation and consistent defect bridging by week 12 (2.5 μg). These doses were specifically chosen to allow for either a positive or negative effect of loading on vascular growth and bone regeneration to be observed. Analysis of vascular growth and regeneration were performed at week 3 postsurgery, a time point identified previously (18), to determine the effect of loading on vascular growth prior to the onset of extensive bone formation.

Vascular growth. Vascular structures in the early loading groups were quantitatively analyzed by microCT angiography at week 3 postsurgery in two 6.3-mm-long cylindrical volumes of interest (VOI): a 5-mm diameter "defect VOI" that contained only the bone defect region and a 7-mm diameter "total VOI" that included both the defect and immediate surrounding soft tissues (Fig. 2*A*). There were no differences in the vascular volume (Fig. 2*B*) or connectivity (a measure of the interconnectedness of the vascular structures, Fig. 2*D*) between groups for the total VOI; however, within the defect VOI, early loading significantly reduced vascular volume (Fig. 2*C*) and connectivity (Fig. 2*E*) by 66% and 91%, respectively, for the 2.5 μg rhBMP-2 dose. Similar trends were found for the 0.5 μg dose, though these differences were not statistically significant ($p = 0.56$ and 0.16 for vascular volume and connectivity, respectively). The vascular volume in the surrounding tissues alone was not significantly affected by fixation plate ($p = 0.17$). Other morphometric parameters including vascular thickness (measure of average vessel diameter), separation (spacing between vessels), number (number of distinct vessels), and degree of anisotropy (indicator of preferential orientation of the vessels) were not significantly altered by loading at either dose for both the total and defect VOI (Fig. S3).

The rhBMP-2 dose was a significant predictor for both vascular volume and connectivity (Fig. 2). Also, within the total VOI, there were no differences between the stiff and compliant plate groups. Therefore, to assess the bone morphogenetic protein (BMP)-mediated vascular response to injury, the stiff and compliant plate groups were pooled based on rhBMP-2 dose and the vascular morphology in the total VOI was compared to age-matched unoperated control limbs ($n = 12$). Defects receiving the larger dose of rhBMP-2 featured significantly enhanced vascular network formation (Fig. S2). Also, the newly formed vascular networks differed significantly from native vascular morphology: the BMP-mediated angiogenic response to injury resulted in increased vascular volume, connectivity, and thickness compared to unoperated controls (Fig. S2 *B–D*); however, whereas native vessels exhibited preferential alignment along the limb axis, the newly formed vascular networks were significantly more isotropic with no preferred orientation in any direction (Fig. S2*E*).

The spatial distribution of blood vessels within the defect VOI was also analyzed by comparing proximal and distal volumes of interest in the stiff plate groups (Fig. S4*A*). The vessel volume, connectivity, and thickness were significantly greater at the proximal end of the defects than at the distal end (Fig. S4 *B–D*, respectively).

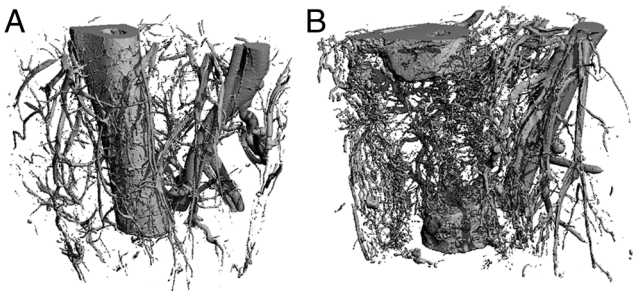

Fig. 1. Vascular response to bone injury: angiogenesis and collateral vessel formation. (*A*) MicroCT image of age-matched unoperated femur with surrounding vasculature. (*B*) Bone and vascular structures 3 wk following creation of an 8 mm bone defect.

Bone regeneration. Consistent with the effects of vascular growth, bone formation within the defect was significantly inhibited by early loading (Fig. 3). Qualitative evaluation of bone formation at week 2 postsurgery was performed by digital X-ray radiography, illustrating reduced bone formation in the compliant plate group at the 2.5 μg dose (Fig. 3*A*). MicroCT reconstructions of undecalcified, contrast agent-perfused samples allowed simultaneous visualization of bone formation and vasculature within the defect region at week 3 postsurgery and confirmed the radiographic observations (Fig. 3*B*). Following subtraction of the vascular volume in the defect, microCT quantification revealed a significant 75% decrease in bone volume in the compliant plate group compared to the stiff plate group at the 2.5 μg rhBMP-2 dose (Fig. 3*C*). As expected, bone volume at the 0.5 μg dose was lower overall than the 2.5 μg dose, and differences between the loading groups at the lower dose were not significant ($p = 0.09$).

Histology. One representative sample from each group was decalcified, embedded in paraffin, and sectioned to 5 μm for histology without contrast agent perfusion. The high eosinophilicity of erythrocytes allowed identification of blood vessels in Haematoxylin and Eosin (H&E) stained sections (Fig. S5). Vessel size and area density were qualitatively consistent with microCT angiography results (Fig. 4*A*). In representative samples analyzed for histology, the stiff plate groups appeared to have more and larger blood vessels than the compliant plate groups.

Interestingly, Safranin-O staining demonstrated that early loading altered tissue-biomaterial interactions (Fig. 4*B*). In the stiff plate groups, formation of connective and mineralized tissues were well-integrated with islands of remnant hydrogel biomaterial; however, in the loaded groups, the predominantly soft tissues that filled the defect failed to adhere to the alginate hydrogel, resulting in void formation around the biomaterial.

The presence of cartilage and endochondral bone formation was also evident in all four groups; however, chondrocyte function appeared to be altered by the mechanical environment (Fig. 4*C*). Chondrocytes were present in both stiff and compliant plate groups, but the dark red staining of glycosaminoglycans (GAG) was more evident in the compliant plate groups. Likewise, the amount of cartilage formation was also qualitatively greater in the compliant plate groups.

Effects of Delayed Mechanical Loading. To evaluate the effects of delayed loading, compliant fixation plates were initially implanted in a locked configuration, but were then unlocked at week 4 postsurgery to allow axial load transfer. Animals were sacrificed for

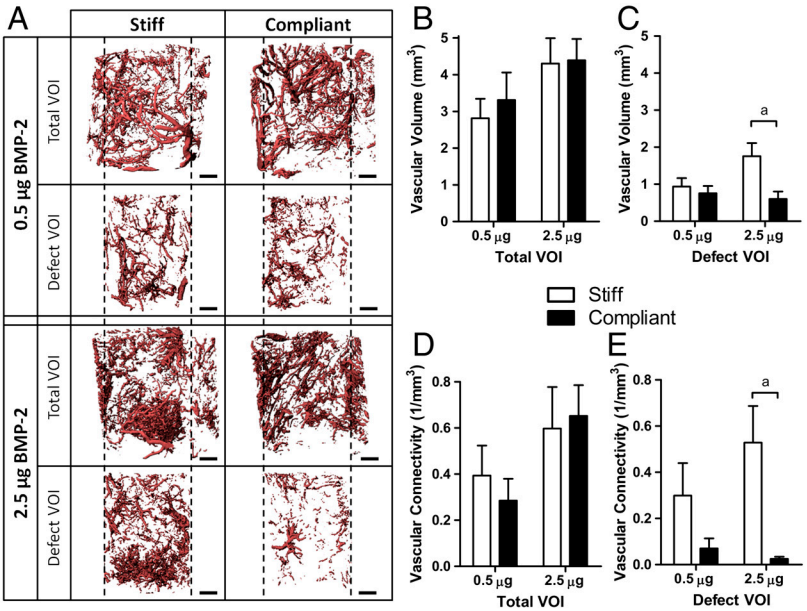

Fig. 2. MicroCT angiography of early loading groups at week 3 postsurgery. Compliant plates were implanted in an unlocked configuration allowing load transfer from day 0. (*A*) Representative 3D reconstructions of vascular structures in the total VOI (7 mm Ø) and defect VOI (5 mm Ø) for each dose and fixation plate type. Scale bars: 1 mm. (*B*, *C*) Vascular volume in total VOI and defect VOI, respectively. (*D*, *E*) Vascular connectivity in the total VOI and defect VOI, respectively. $N = 9$–10 per group; (*a*) $p < 0.05$.

analysis at week 7 postsurgery, 3 wk after load initiation. Defects in the delayed loading group and their contralateral stiff plate controls ($n = 11$–12 per group) each received 5.0 μg rhBMP-2, which induces consistent bridging of the defects by week 4, the time point of compliant plate unlocking (19). The dose of rhBMP-2 was increased from 2.5 to 5.0 μg to induce consistent bridging of the defects by week 4, the time of compliant plate unlocking (19).

Vascular growth. Vascular structures in the delayed loading groups at week 7 were quantified by microCT angiography in both the defect VOI and total VOI (Fig. 5). There were no differences in vascular volume between the stiff and compliant plate groups for either total or defect VOI (Fig. 5*B*); however, vascular connectivity (Fig. 5*C*) and vascular number (Fig. 5*D*) were significantly lower in the compliant plate group for both total and

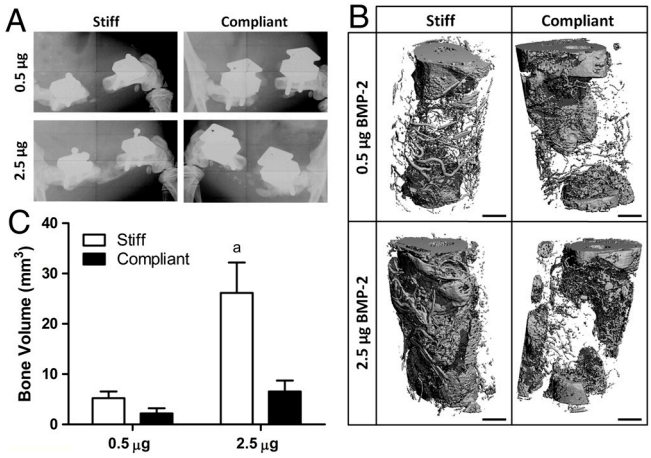

Fig. 3. Digital X-ray and microCT evaluation of bone formation in early loading groups, in which the compliant plates were unlocked prior to implantation. (*A*) Radiographs of limbs at week 2 postsurgery. (*B*) MicroCT reconstructions of undecalcified perfused samples at week 3 postsurgery showing both bone formation and vascular growth. Scale bars: 1 mm. (*C*) Quantification of bone volume. $N = 8$–9 per group; (*a*) $p < 0.05$ vs. all other groups.

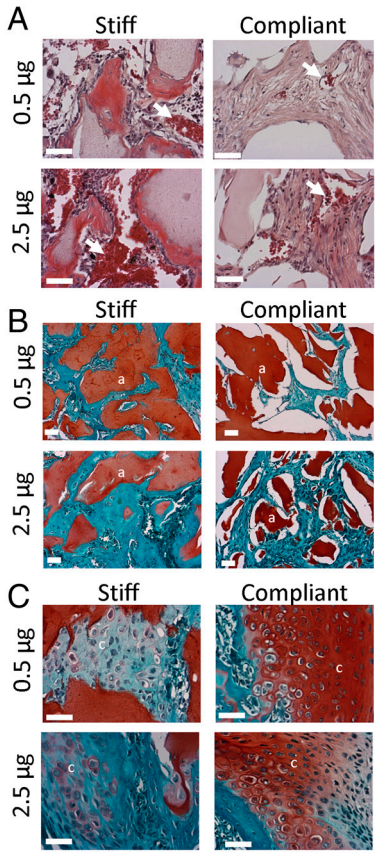

Fig. 4. Week 3 histological staining of sagittal sections of early loading groups, in which the compliant plates were unlocked prior to implantation. (*A*) H&E-stained sections allowed identification of blood vessels by dark staining of erythrocytes (white arrows). Images at 20×. (*B*) Safranin-O/fast-green-stained sections illustrating disruption of alginate (*a*) integration with surrounding tissues (blue-green). Images at 10×. (*C*) Safranin-O/fast-green-stained sections illustrating cartilage (*c*) and endochondral bone formation. Images at 20×. All scale bars: 50 μm.

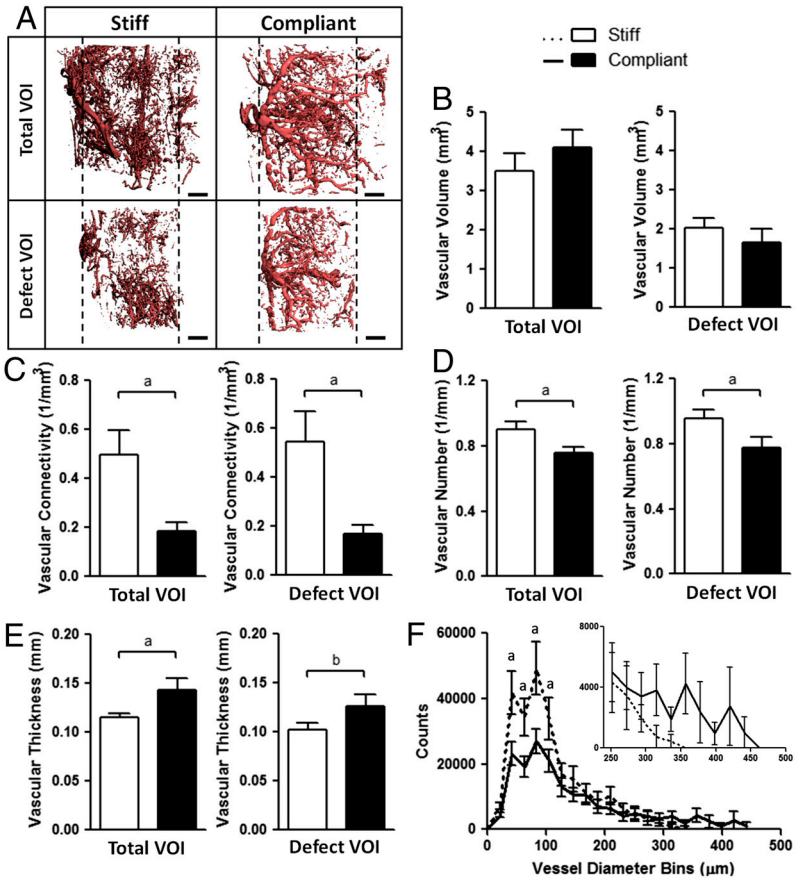

Fig. 5. MicroCT angiography of delayed loading groups at week 7 postsurgery. Compliant plates were initially implanted in the locked configuration, but were unlocked at week 4, allowing load transfer for a further 3 wk. (*A*) Representative 3D reconstructions of vascular structures in the total VOI (7 mm Ø) and defect VOI (5 mm Ø) for both fixation plate types. Scale bars: 1 mm. (*B–E*) Vascular morphology parameters in the total and defect VOIs: vascular volume (*B*), vascular connectivity (*C*), vascular number (*D*), and vascular thickness (*E*). (*F*) Vascular thickness histogram indicating blood vessel size distribution. (*Inset*) Magnification of 252–462 μm bins. $N = 11$–12 per group; (*a*) $p < 0.05$; (*b*) $p = 0.08$.

defect VOIs. Whereas differences in vascular thickness did not reach significance in the defect VOI ($p = 0.08$), the compliant plate group had a significantly greater vascular thickness in the total VOI (Fig. 5*E*). In the defect VOI, the frequency distribution of vessel diameters indicated a significantly lower number of small diameter vessel bins (40–100 μm in diameter; Fig. 5*F*) and an extension of large diameter vessel bins (315–441 μm in diameter; Fig. 5*F*, inset) in the compliant plate group. Delayed loading also significantly decreased vascular separation in both VOIs but did not alter degree of anisotropy (Fig. S6).

Bone regeneration. In contrast to the effects of early loading, delayed mechanical loading significantly enhanced bone formation (Fig. 6). Digital radiography revealed that all defects had bridged with bone prior to plate unlocking at week 4, and at this time the stiff and compliant plate groups featured similar bone formation. At week 7, however, after 3 wk of loading, there appeared to be denser bone formation in the compliant plate group (Fig. 6*A*). Postmortem microCT analysis allowed reconstruction of the combined bone and vascular structures (Fig. 6*B*) and, following subtraction of vascular volumes, revealed a significant 20% increase in bone volume in the mechanically loaded group at week 7 (Fig. 6*C*).

Histology. One representative sample per group was selected prior to perfusion for histological staining. H&E and Safranin-O staining at week 7 revealed substantial osteocyte-populated woven bone formation and strong integration of newly formed bone with regions of alginate gel (Fig. 7 *A* and *B*). Individual hypertrophic chondrocytes and small remnants of endochondral bone formation were evident in both groups, with more chondrocytes remaining in the compliant plate group (Fig. 7*C*).

Discussion

The results of this study indicate that neovascular network formation and growth are regulated by mechanical conditions in vivo, and surrounding matrix deformations alter vessel formation and remodeling, to regulate engineered tissue regeneration. These data also suggest that the timing and magnitude of loading are important variables that warrant further research to determine an optimal window of therapeutic effect. Recently, Kilarski et al. demonstrated that endogenous fibroblasts and myofibroblasts recruited during wound healing exert tensile stresses that regulate nonangiogenic expansion of blood vessels into fibrinogen/collagen scaffolds implanted onto chick chorioallantoic membranes (23). In that study, however, mechanical conditions were neither measured nor directly controlled. The present study demonstrates that in vivo biomechanical stimulation may diminish or enhance vascularization of engineered tissues, depending on the time of application during the healing process.

Early mechanical loading inhibited vascular ingrowth into the defect, but did not change the overall angiogenic response to injury: the vessel volume and connectivity in the total VOI were not altered, suggesting that loading had a localized effect that inhibited ingrowth of vessels into the defect. These inhibitory effects were likely due to excessive interfragmentary motion associated with loading prior to defect stabilization by bone formation. In native bone tissue, matrix strains typically reach 0.3% (24); however, under the loading conditions determined for this

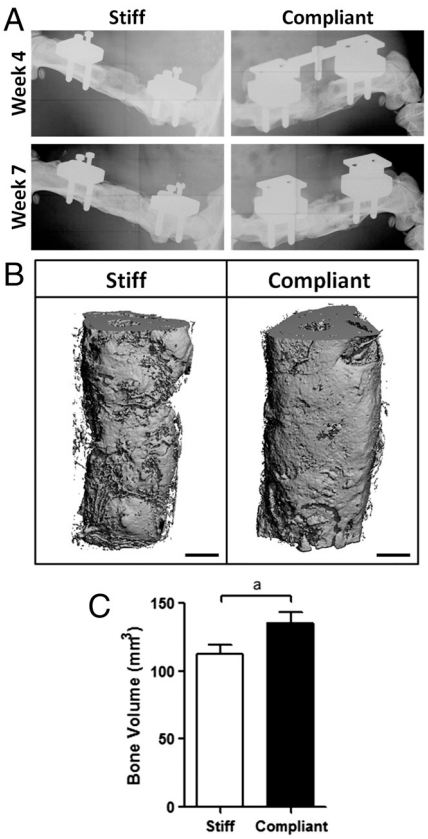

Fig. 6. Digital X-ray and microCT evaluation of bone formation in delayed loading groups, in which the compliant plates were unlocked at week 4 postsurgery. (*A*) Radiographs of limbs at weeks 4 and 7 postsurgery. (*B*) MicroCT reconstructions of undecalcified, perfused samples at week 7 postsurgery showing both bone formation and vascular growth. Scale bars: 1 mm. (*C*) Quantification of bone volume alone. $N = 10–11$ per group; (*a*) $p < 0.05$.

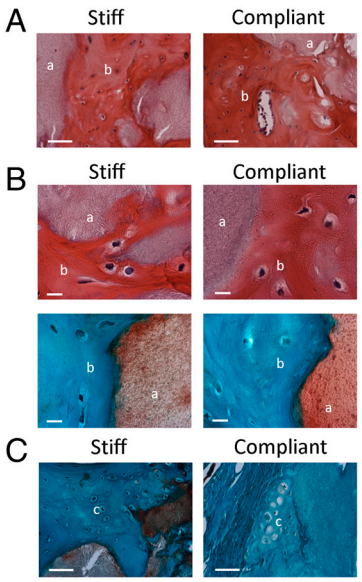

Fig. 7. Week 7 histological staining of sagittal sections of delayed loading groups, in which the compliant plates were unlocked at week 4 postsurgery. (*A*) H&E-stained sections illustrate bone formation (*b*) and regions of alginate (*a*). Images at 20×; scale bars: 50 μm. (*B*) H&E (*Upper*) and Safranin-O/fast-green-stained (*Lower*) sections illustrating bone and alginate integration. Images at 63×; scale bars: 10 μm. (*C*) Safranin-O/fast-green-stained sections illustrating remnants of cartilage (*c*) and endochondral bone formation. Images at 20×; scale bars: 50 μm.

model, early loading resulted in initial axial interfragmentary strains of 5–10%, assuming negligible contribution of the mesh/alginate construct to defect stability. It was these relatively large initial strains that likely inhibited blood vessel ingrowth and bone formation in the compliant plate groups. In addition to disrupting vascular invasion, which inhibited bone formation, early deformations within the defect may have promoted tissue differentiation toward more fibrotic and cartilaginous tissue types, which are inherently less vascularized. Perren et al. and Carter et al. proposed this explanation to explain the effects of loading on bone fracture callus differentiation (25, 26). Finally, early mechanical loading may have accelerated rhBMP-2 release, depleting signals that would promote regeneration. For example, Lee et al. demonstrated an accelerated release of growth factors from alginate hydrogels under mechanical stimulation (27). Together, these data point to the importance of limiting mechanical deformations during the initial phase of vascular ingrowth but do not rule out the potential for more moderate mechanical conditions to stimulate tissue regeneration early in the healing the process.

Qualitative differences in cartilage matrix production were observed as a result of early loading. Though cartilage was present in all groups at week 3 postsurgery, loading appeared to increase or prolong GAG production, as indicated by the intensity of Safranin-O staining. This is consistent with reports in the literature that mechanical loading prolongs the chondral phase of endochondral ossification in defect healing (28). Also, we have previously observed greater bone formation at the proximal ends of the defects in this model. We hypothesized that these differences were to due to reduced vascular supply at the distal end of the defects. This study confirmed this hypothesis, showing a significantly lower vascular volume, connectivity and thickness at the distal end of the defects compared to the proximal end. The reason for this spatial variation in vascular invasion may be attributed to the greater surrounding soft tissue coverage at the proximal end.

Independent of loading conditions, vascular growth responded in a dose-dependent manner to rhBMP-2 by week 3. The mechanisms by which rhBMP-2 may induce vascular growth remain unclear, but reports of direct angiogenic effects on endothelial cells (29, 30) and paracrine upregulation of VEGF expression in osteoblasts (31) have been reported. Overall, the vascular response to injury resulted in networks with greater volume, connectivity and isotropy than native uninjured tissue.

Application of delayed mechanical loading significantly enhanced bone formation. Unlike early loading, it also allowed growth of blood vessels into the defect, but did not stimulate angiogenesis, as evidenced by the equivalent vascular volume in the stiff and compliant plate groups. However, the delayed loading treatment did induce vascular remodeling, reducing vascular number and connectivity and increasing vessel thickness, with a reduction in the number of small vessels (40–100 μm in diameter) and an expansion in the number of large vessels (315–441 μm in diameter). Although not directly measured, the observed adaptation in vascular network architecture may have served to enhance perfusion efficiency within the defect by pruning smaller vessels and increasing the average thickness of remaining vessels.

Together, these data suggest that delayed mechanical loading stimulates vascular remodeling through arteriogenesis, the growth and dilation of existing arterioles by proliferation of endothelial and smooth muscle cells (32). These results are consistent with previous observations of vascular remodeling in rodent models of hindlimb ischemia, which have shown that whereas angiogenesis is governed primarily by tissue ischemia, arteriogenesis is likely regulated by biomechanical factors including luminal shear and vessel strain (22, 33, 34). Similarly, Cao et al. (35) demonstrated that the transition between maintenance and regression of new vessels is dependent on exposure to growth factors at the time of vessel birth, and these same factors (PDGF, FGF, and VEGF), are regulated by mechanical conditions (5, 36–38). Thus,

delayed mechanical loading may have accelerated the maturation and remodeling of new vessels, and thereby enhanced tissue regeneration.

These experiments cannot uncouple the effects of mechanical forces on vascular growth and tissue formation and differentiation. Osteogenesis and angiogenesis are linked on a molecular level, and it is not possible to induce bone formation without vascular ingrowth (13). In growth plate development, for example, expression of angiogenic factors precedes vessel formation, chondrocyte hypertrophy, and ultimately bone formation (39). Regulation of the genes and signaling molecules important for the genesis of cartilage, bone, and vasculature, such as Indian Hedgehog (Ihh), Runx2, and VEGF, respectively, are shared such that knock-out animals lacking any of these three genes experience defects in each of the three tissues, suggesting a fundamental link between tissue formation and vascular growth (39). These observations highlight the importance of conducting functional in vivo studies in addition to isolated in vitro experiments.

An alternative interpretation of the data is that delayed loading may have induced remodeling simply by disrupting small vessel formation, which in turn reduced connectivity and vascular number, without disrupting the larger vessels that had developed prior to the onset of loading, allowing sufficient vascular supply for bone formation. However, loading also increased the number of large vessels in the defect region. Further, the observed enhancements in bone formation suggest an increased vascular demand, requiring an improved functional network. This is consistent with reports in the literature that in vitro mechanical loading primarily alters vascular remodeling over angiogenesis (8–10, 40). Likewise, beneficial effects of loading on vascular growth have been observed in the bone fracture healing literature (37). Further research is warranted to elucidate these adaptive mechanisms, as such insight would have important implications for the engineering of many vascularized tissues.

Delayed loading did not impair tissue-biomaterial integration, though it may have regulated tissue differentiation by prolonging endochondral bone formation and cartilage hypertrophy, consistent with previous observations (28). These findings suggest that the mechanical environment is an important regulator of engineered tissue formation and differentiation.

Conclusions

This study quantified the effects of early and delayed mechanical loading on neovascular growth and remodeling and tissue regeneration in vivo. Whereas early loading disrupted neovascular ingrowth and prevented bone formation, delayed loading stimulated vascular network remodeling and enhanced bone regeneration. Together, these data demonstrate the mechanosensitivity of neovascular networks in vivo and highlight the capacity of mechanical stimulation to modulate postnatal vascular growth and remodeling.

Materials and Methods

Surgical Procedure. Bilateral 8-mm bone defects were surgically created in femora of 13-wk-old female Sasco SD rats (Charles River Labs), as previously described (17, 21). Limbs were stabilized by either stiff fixation plates or compliant plates that could be unlocked to allow transfer of ambulatory loads, but constrained the loading along the bone axis ($n = 10$–12 per group) (21). The stiff plates featured an axial stiffness of 214.3 ± 4.1 N/mm, whereas the compliant plates had a stiffness of 349.5 ± 35.1 N/mm and 8.4 ± 0.4 N/mm in the locked and unlocked configurations, respectively (21). All defects were treated with rhBMP-2, delivered in a hybrid nanofiber mesh/alginate delivery system, as described previously (18). See *SI Materials and Methods* for details. Defects in the early loading groups and their contralateral controls received either 0.5 or 2.5 μg rhBMP-2; defects in the delayed loading group and their stiff plate controls received 5.0 μg rhBMP-2 (Table S1). Previous studies have demonstrated that in the absence of BMP, the defect contains very little bone formation or vascular ingrowth (18, 19). All procedures were approved by the Georgia Institute of Technology Institutional Animal Care and Use Committee (protocol #A08032).

Faxitron. Digital radiographs (Faxitron MX-20 Digital; Faxitron X-ray Corp.) were performed at an exposure time of 15 s and a voltage of 25 kV. Animals from the early loading groups ($n = 9$–10 per group), received X-ray imaging at week 2 postsurgery. Animals from the delayed loading groups ($n = 11$–12 per group) were imaged at weeks two, four, and seven postsurgery.

MicroCT Angiography. Eight to eleven samples from each group were reserved for microCT angiography. All animals were euthanized by CO_2 asphyxiation 3 wk after compliant plate unlocking: Early loading groups were euthanized at week 3 and delayed loading groups were euthanized at week 7. Radiopaque contrast agent-enhanced microCT angiography was performed using a protocol modified from Duvall et al. (22). See *SI Materials and Methods* for details. Briefly, the vasculature was perfused through the ascending aorta with sequential solutions of vasodilator, saline, neutral buffered formalin, and lead chromate-based radiopaque contrast agent (Microfil MV-122, Flow Tech).

MicroCT Analysis. MicroCT scans (VivaCT 40, Scanco Medical) were performed at 21.0 μm voxel size at a voltage of 55 kVp and a current of 109 μA. Tissues were segmented by application of a global threshold corresponding to 386 mg hydroxyapatite/cm^3, and a low-pass Gaussian filter (sigma = 1.2, support = 1) was used to suppress noise. Following initial microCT scanning to evaluate both new bone and perfused vessels, samples were transferred to a formic acid-based decalcifying agent (Cal-ExII, Fisher Scientific or Immunocal, Decal Chemical Co.) for 2–3 wk. Decalcified samples were then rescanned using the same settings and in the same position as before to quantify vascular structures alone.

Two 6.3-mm-long cylindrical VOI were contoured for analysis: a defect VOI (5 mm diameter) and a total VOI (7 mm diameter). The defect VOI encompassed only the nanofiber mesh and defect region, whereas the total VOI included the defect and surrounding soft tissues. The position of the VOIs in the pre- and postdecalcification scans was registered to the fixation plate. For predecalcification analysis, the volume of all attenuating tissues, including bone and contrast agent-filled vasculature was computed. After decalcification, the vascular volume, connectivity, thickness, thickness frequency distribution, number, separation, and degree of anisotropy were analyzed as described previously (22). The bone volume in the defect was then computed by subtraction of the vascular volume from the predecalcified volume in the total VOI. The vascular morphology was compared between the proximal and distal ends of the defects by separately analyzing each half of the defect VOI (5 mm diameter × 3.15 mm length) in the stiff plate groups.

Histology. One representative sample per group was chosen for histology based on qualitative Faxitron evaluation of bone growth. Samples were fixed in 10% neutral buffered formalin for 48 h at 4 °C and then decalcified over 2 wk under mild agitation on a rocker plate. Following paraffin processing, 5 μm-thick midsagittal sections were cut and stained with H&E or Safranin-O/Fast-green (41).

Statistical Analyses. All data are presented as mean ± standard error of the mean (SEM). Differences between groups, accounting for animal variability, were assessed by analysis of variance (ANOVA) with pairwise comparisons made by Tukey's post hoc analysis. A p-value < 0.05 was considered significant. Minitab® 15 (Minitab Inc.) was used to perform the statistical analysis.

ACKNOWLEDGMENTS. We thank Dr. David Mooney for discussions regarding the delivery system, and Dr. Laura O'Farrell for assistance with animal studies. We also thank Dr. Tamim Diab, Angela Lin, Hazel Stevens, Christopher Dosier, Mon Tzu Li, Tanushree Thote, and Ashley Allen for their assistance in surgeries. This work was supported by grants from the National Institutes of Health, the Armed Forces Institute for Regenerative Medicine, and the US Department of Defense.

1. Koike N, et al. (2004) Tissue engineering: Creation of long-lasting blood vessels. *Nature* 428:138–139.
2. Kannan RY, Salacinski HJ, Sales K, Butler P, Seifalian AM (2005) The roles of tissue engineering and vascularisation in the development of micro-vascular networks: A review. *Biomaterials* 26:1857–1875.
3. Duncan RL, Turner CH (1995) Mechanotransduction and the functional response of bone to mechanical strain. *Calcif Tissue Int* 57:344–358.
4. Tschumperlin DJ, et al. (2004) Mechanotransduction through growth-factor shedding into the extracellular space. *Nature* 429:83–86.

5. Yung YC, Chae J, Buehler MJ, Hunter CP, Mooney DJ (2009) Cyclic tensile strain triggers a sequence of autocrine and paracrine signaling to regulate angiogenic sprouting in human vascular cells. *Proc Natl Acad Sci USA* 106:15279–15284.
6. Robling AG, Castillo AB, Turner CH (2006) Biomechanical and molecular regulation of bone remodeling. *Annu Rev Biomed Eng* 8:455–498.
7. Ando J, Nomura H, Kamiya A (1987) The effect of fluid shear stress on the migration and proliferation of cultured endothelial cells. *Microvasc Res* 33:62–70.
8. Matsumoto T, et al. (2007) Mechanical strain regulates endothelial cell patterning in vitro. *Tissue Eng* 13:207–217.
9. Krishnan L, et al. (2008) Effect of mechanical boundary conditions on orientation of angiogenic microvessels. *Cardiovasc Res* 78:324–332.
10. Joung IS, Iwamoto MN, Shiu YT, Quam CT (2006) Cyclic strain modulates tubulogenesis of endothelial cells in a 3D tissue culture model. *Microvasc Res* 71:1–11.
11. Mammoto A, et al. (2009) A mechanosensitive transcriptional mechanism that controls angiogenesis. *Nature* 457:1103–1108.
12. Wilson CJ, Kasper G, Schutz MA, Duda GN (2009) Cyclic strain disrupts endothelial network formation on Matrigel. *Microvasc Res* 78:358–363.
13. Street J, et al. (2002) Vascular endothelial growth factor stimulates bone repair by promoting angiogenesis and bone turnover. *Proc Natl Acad Sci USA* 99:9656–9661.
14. Claes L, Eckert-Hubner K, Augat P (2002) The effect of mechanical stability on local vascularization and tissue differentiation in callus healing. *J Orthop Res* 20: 1099–1105.
15. Griffith LG, Naughton G (2002) Tissue engineering—current challenges and expanding opportunities. *Science* 295:1009–1014.
16. Rai B, et al. (2007) Combination of platelet-rich plasma with polycaprolactone-tricalcium phosphate scaffolds for segmental bone defect repair. *J Biomed Mater Res A* 81:888–899.
17. Oest ME, Dupont KM, Kong HJ, Mooney DJ, Guldberg RE (2007) Quantitative assessment of scaffold and growth factor-mediated repair of critically sized bone defects. *J Orthop Res*.
18. Kolambkar YM, et al. (2011) An alginate-based hybrid system for growth factor delivery in the functional repair of large bone defects. *Biomaterials* 32:65–74.
19. Boerckel JD, et al. (2011) Effects of protein dose and delivery system on BMP-mediated bone regeneration. *Biomaterials* 32:5241–5251.
20. Kolambkar YM, et al. (2011) Spatiotemporal delivery of bone morphogenetic protein enhances functional repair of segmental bone defects. *Bone* 49:485–492.
21. Boerckel JD, Dupont KM, Kolambkar YM, Lin AS, Guldberg RE (2009) In vivo model for evaluating the effects of mechanical stimulation on tissue-engineered bone repair. *J Biomech Eng* 131:084502.
22. Duvall CL, Taylor WR, Weiss D, Guldberg RE (2004) Quantitative microcomputed tomography analysis of collateral vessel development after ischemic injury. *Am J Physiol Heart Circ Physiol* 287:H302–310.
23. Kilarski WW, Samolov B, Petersson L, Kvanta A, Gerwins P (2009) Biomechanical regulation of blood vessel growth during tissue vascularization. *Nat Med* 15:657–664.
24. Cowin SC, Doty SB (2007) *Tissue Mechanics* (Springer, New York) p 385.
25. Perren SM, Cordey J (1980) *The Concept of Interfragmentary Strain* (Springer, Berlin).
26. Carter DR, Beaupre GS, Giori NJ, Helms JA (1998) Mechanobiology of skeletal regeneration. *Clin Orthop Relat Res* 355s:S41–S55.
27. Lee KY, Peters MC, Anderson KW, Mooney DJ (2000) Controlled growth factor release from synthetic extracellular matrices. *Nature* 408:998–1000.
28. Epari DR, Schell H, Bail HJ, Duda GN (2006) Instability prolongs the chondral phase during bone healing in sheep. *Bone* 38:864–870.
29. Moutsatsos IK, et al. (2001) Exogenously regulated stem cell-mediated gene therapy for bone regeneration. *Mol Ther* 3:449–461.
30. Langenfeld EM, Langenfeld J (2004) Bone morphogenetic protein-2 stimulates angiogenesis in developing tumors. *Mol Cancer Res* 2:141–149.
31. Deckers MM, et al. (2002) Bone morphogenetic proteins stimulate angiogenesis through osteoblast-derived vascular endothelial growth factor A. *Endocrinology* 143:1545–1553.
32. van Royen N, Piek JJ, Schaper W, Fulton WF (2009) A critical review of clinical arteriogenesis research. *J Am Coll Cardiol* 55:17–25.
33. Scholz D, et al. (2002) Contribution of arteriogenesis and angiogenesis to postocclusive hindlimb perfusion in mice. *J Mol Cell Cardiol* 34:775–787.
34. Egginton S (2009) Invited review: Activity-induced angiogenesis. *Pflugers Arch* 457: 963–977.
35. Cao R, et al. (2003) Angiogenic synergism, vascular stability and improvement of hindlimb ischemia by a combination of PDGF-BB and FGF-2. *Nat Med* 9:604–613.
36. Barron MJ, Tsai CJ, Donahue SW (2010) Mechanical stimulation mediates gene expression in MC3T3 osteoblastic cells differently in 2D and 3D environments. *J Biomech Eng* 132:041005.
37. Groothuis A, et al. (2010) Mechanical stimulation of the pro-angiogenic capacity of human fracture haematoma: involvement of VEGF mechano-regulation. *Bone* 47: 438–444.
38. Clarke MS, Feeback DL (1996) Mechanical load induces sarcoplasmic wounding and FGF release in differentiated human skeletal muscle cultures. *FASEB J* 10:502–509.
39. Colnot C, et al. (2005) Indian hedgehog synchronizes skeletal angiogenesis and perichondrial maturation with cartilage development. *Development* 132:1057–1067.
40. Matsumoto T, et al. (2007) Three-dimensional cell and tissue patterning in a strained fibrin gel system. *PLoS One* 2:e1211.
41. Rosenberg L (1971) Chemical basis for the histological use of safranin O in the study of articular cartilage. *J Bone Joint Surg Am* 53:69–82.

Supporting Information

Boerckel et al. 10.1073/pnas.1107019108

SI Materials and Methods.

Surgical Procedure. Bilateral, critically sized (8 mm) bone defects were surgically created in femora of 13-wk-old female Sasco Sprague–Dawley rats (Charles River) as previously described (1, 2). Limbs were stabilized by either stiff fixation plates or compliant plates that allowed elective actuation of axial load sharing (1) ($n = 10$–12 per group). The stiff plates featured an axial stiffness of 214.3 ± 4.1 N/mm, whereas the compliant plates had a stiffness of 349.5 ± 35.1 N/mm and 8.4 ± 0.4 N/mm in the locked and actuated configurations, respectively (1). Compliant fixation plates were actuated to allow ambulatory load transfer either at the time of initial implantation (early loading group) or at week 4 postsurgery (delayed loading group). Animals from each group received a compliant fixation plate and a contralateral stiff plate control. Animals in the delayed loading group received a secondary operation to actuate the compliant plates at week 4 postsurgery, whereas contralateral stiff plate controls were sham operated at the same time.

Mesh/Alginate Delivery System. All defects were treated with recombinant human bone morphogenetic protein-2 (rhBMP-2), delivered in a hybrid nanofiber mesh/alginate-based delivery system (3). Briefly, perforated nanofiber mesh tubes were created as described previously and were placed over the native bone ends, surrounding the defect (3). One hundred fifty microliters of alginate hydrogel containing the appropriate dose of rhBMP-2 was then injected into the defect space (3). Defects in the early loading group and their contralateral controls received either 0.5 or 2.5 μg rhBMP-2. Defects in the delayed loading group and their stiff plate controls received 5.0 μg rhBMP-2, resulting in the six groups illustrated in Table S1. The doses were chosen based on a previous dose-response study (4). In the early loading study, two doses were chosen: one that induces bone formation, but fails to induce consistent bridging of the defects (0.5 μg), and one that induces robust bone formation and consistent defect bridging by week 12, without oversaturating the response (2.5 μg). These doses were chosen to allow for either a positive or negative effect of loading on vascular growth. For the delayed loading study, we chose a dose (5.0 μg) that induced consistent bridging of the defects at week 4, the time point of compliant plate actuation. The 2.5 microgram dose was not used as it fails to induce consistent bridging of the defects by week 4 (bridging rate: 60%) (4). The absence of bridging would drastically influence the amount of interfragmentary motion compared with bridged defects.

Recombinant human BMP-2 (R&D Systems) was reconstituted in 0.1% rat serum albumin in 4 mM HCl, according to manufacturer instructions. The rhBMP-2 was then mixed with RGD (Arg–Gly–Asp) peptide-functionalized alginate (5–7) to a final concentration of 2% alginate, which was crosslinked by rapidly mixing with 0.84% (m/v) $CaSO_4$. Each defect received 150 μL of the pregelled alginate with 0.5, 2.5, or 5.0 μg rhBMP-2, depending on group (Table S1).

MicroCT Angiography. Eight to 11 samples from each group (Table S1) were reserved for microcomputed tomography (microCT) angiography. All animals were euthanized by CO_2 asphyxiation 3 wk after compliant plate actuation: early loading groups were euthanized at week 3 and delayed loading groups were euthanized at week 7. Radiopaque contrast agent-enhanced microCT angiography was performed using a protocol modified from Duvall et al. (8). Briefly, a 2-inch 18-gauge catheter (SURFLO® Teflon IV Catheter, Terumo Medical) was inserted into the left ventricle of the heart and advanced into the ascending aorta. 0.9% saline containing 0.4% (w/v) papaverin hydrochloride (Sigma–Aldrich) was perfused through the vasculature using a peristaltic pump until complete clearance. The vasculature was then fixed in an open configuration by perfusion with 10% neutral buffered formalin (NBF) and cleared with saline. Finally, 25 mL of polymerizable, lead chromate-based, radiopaque contrast agent (Microfil MV-122, Flow Tech) was injected using a 30 mL syringe. The contrast agent was prepared according to manufacturer instructions but diluted to a concentration of 66% to allow simultaneous segmentation of both newly formed bone and vascular contrast agent. Samples were stored at 4 °C for 24 h to allow polymerization of the contrast agent. Hindlimbs were then excised and stored in 10% NBF for 1 wk until preliminary microCT analysis.

1. Boerckel JD, Dupont KM, Kolambkar YM, Lin AS, Guldberg RE (2009) In vivo model for evaluating the effects of mechanical stimulation on tissue-engineered bone repair. *J Biomech Eng* 131:084502.
2. Oest ME, Dupont KM, Kong HJ, Mooney DJ, Guldberg RE (2007) Quantitative assessment of scaffold and growth factor-mediated repair of critically sized bone defects. *J Orthop Res* 25:941–950.
3. Kolambkar YM, et al. (2011) An alginate-based hybrid system for growth factor delivery in the functional repair of large bone defects. *Biomaterials* 32:65–74.
4. Boerckel JD, et al. (2011) Effects of protein dose and delivery system on BMP-mediated bone regeneration. *Biomaterials* 32:5241–5251.
5. Simmons CA, Alsberg E, Hsiong S, Kim WJ, Mooney DJ (2004) Dual growth factor delivery and controlled scaffold degradation enhance in vivo bone formation by transplanted bone marrow stromal cells. *Bone* 35:562–569.
6. Alsberg E, et al. (2003) Regulating bone formation via controlled scaffold degradation. *J Dent Res* 82:903–908.
7. Alsberg E, Anderson KW, Albeiruti A, Franceschi RT, Mooney DJ (2001) Cell-interactive alginate hydrogels for bone tissue engineering. *J Dent Res* 80:2025–2029.
8. Duvall CL, Taylor WR, Weiss D, Guldberg RE (2004) Quantitative microcomputed tomography analysis of collateral vessel development after ischemic injury. *Am J Physiol Heart Circ Physiol* 287:H302–H310.

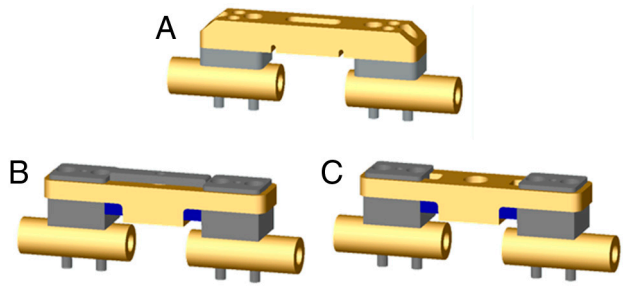

Fig. S1. Fixation plate designs. (*A*) Stiff plate. (*B*) Locked compliant plate. (*C*) Actuated compliant plate.

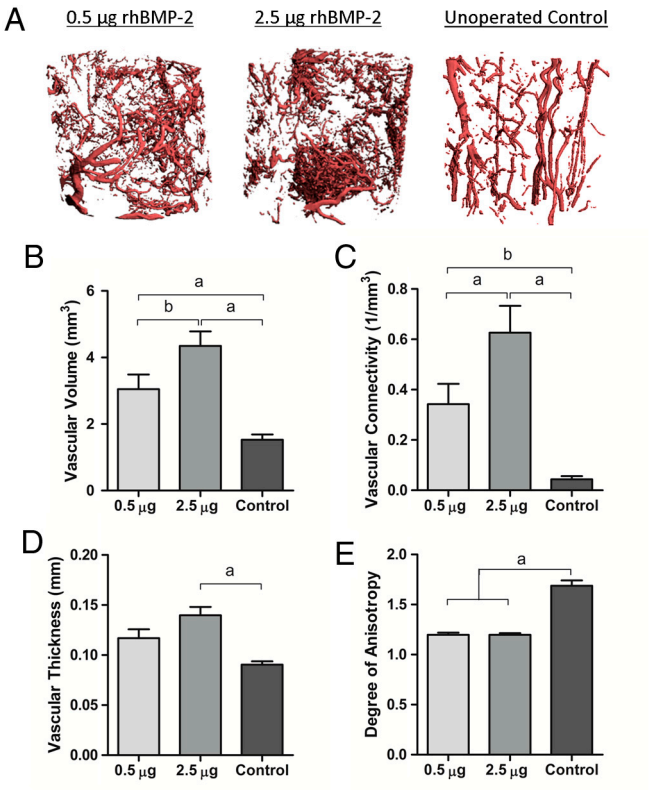

Fig. S2. BMP-mediated vascular response to bone injury. (*A*) Representative total volumes of interest (VOI) images of pooled stiff and compliant plate groups at each dose and age-matched unoperated controls. (*B*) Vascular volume. (*C*) Vascular connectivity. (*D*) Vascular thickness. (*E*) Degree of anisotropy; (*a*) $p < 0.05$, (*b*) $p < 0.053$.

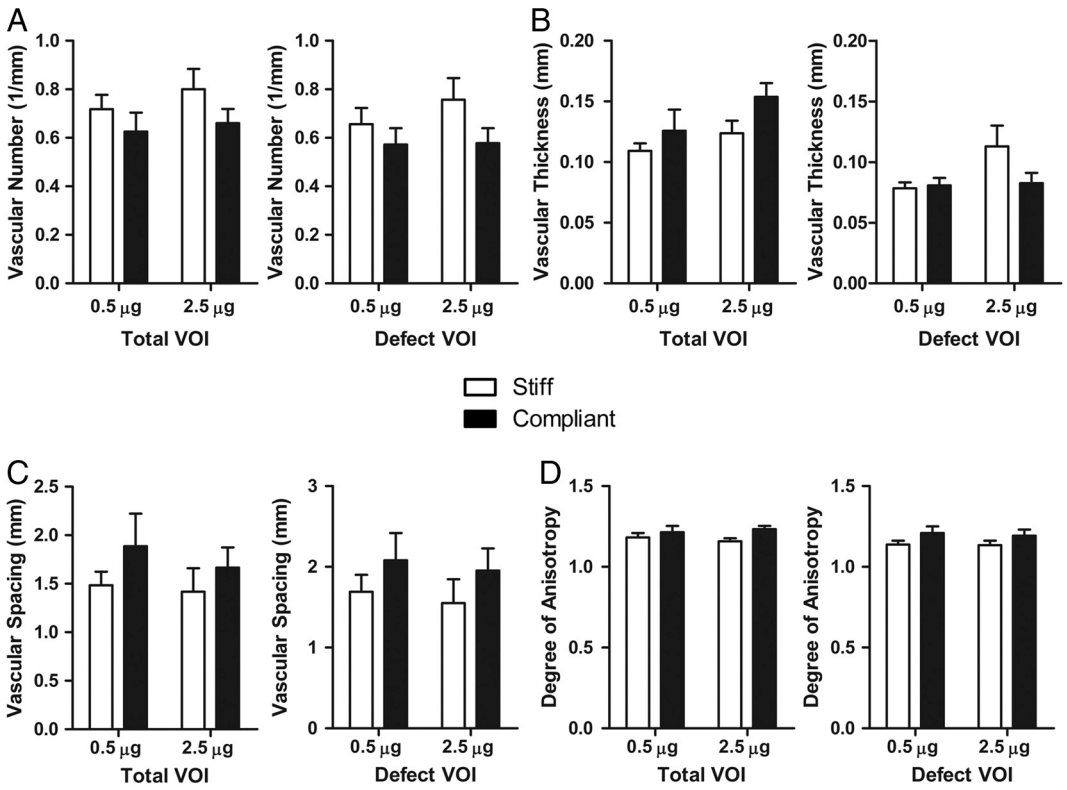

Fig. S3. Vascular morphology parameters not altered by early loading. (*A*) Vascular number. (*B*) Vascular thickness. (*C*) Vascular spacing. (*D*) Degree of anisotropy.

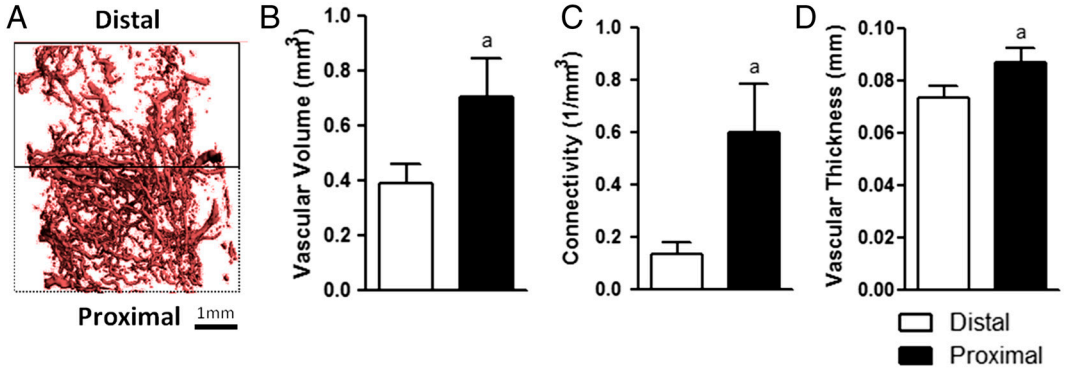

Fig. S4. Spatial inhomogeneity of vessel distribution in the defect VOI of the stiff plate group. (*A*) Representative perfused image showing proximal and distal regions of the defect. (*B–D*) Vascular volume (*B*), vascular connectivity (*C*), and vascular thickness (*D*) in the distal and proximal regions; (*a*) $p < 0.05$ vs. distal region.

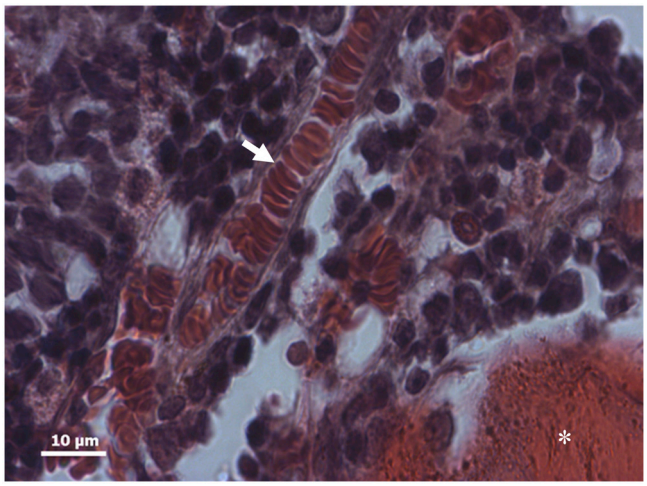

Fig. S5. A 63× magnification image of H&E-stained section showing erythrocytes (white arrow) inside a capillary. The * indicates bone formation.

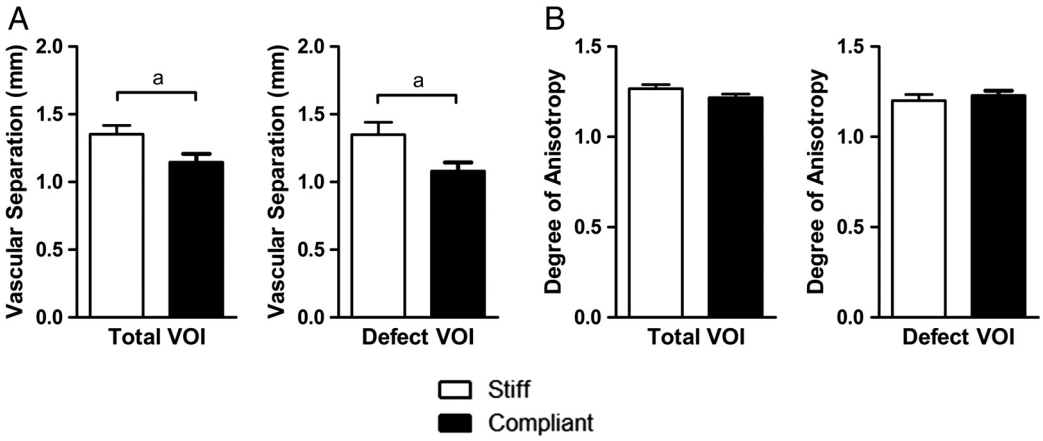

Fig. S6. Vascular morphology parameters. (*A*) Vascular separation. (*B*) Degree of anisotropy. a: $p < 0.05$.

Table S1. Sample sizes for groups and analyses performed

Experiment	Fixation plate	BMP dose	Time of load actuation	Sample sizes for analyses performed						
				Faxitron			MicroCT		Histology	
				Week 2	Week 4	Week 7	Week 3	Week 7	Week 3	Week 7
Early	Stiff	0.5	—	10	—	—	9	—	1	—
Early	Compliant	0.5	Day 0	9	—	—	8	—	1	—
Early	Stiff	2.5	—	9	—	—	8	—	1	—
Early	Compliant	2.5	Day 0	10	—	—	9	—	1	—
Delayed	Stiff	5.0	Sham day 28	12	12	12	—	11	—	1
Delayed	Compliant	5.0	Day 28	11	11	11	—	10	—	1